A new predictive neural architecture for modelling electric field patterns in microwave-heating processes

J.L. Pedreño-Molina* and J. Monzó-Cabrera

Department of Information Technologies and Communications,
Technical University of Cartagena, Campus Muralla del Mar s/n,
E-30.202, Cartagena, Murcia, Spain
E-mail: juan.pmolina@upct.es E-mail: juan.monzo@upct.es
*Corresponding author

M. Pinzolas

Department of Systems Engineering and Automation,
Technical University of Cartagena, Campus Muralla del Mar s/n,
E-30.202, Cartagena, Murcia, Spain
E-mail: miguel.pinzolas@upct.es

M.E. Requena Pérez

Department of Information Technologies and Communications,
Technical University of Cartagena, Campus Muralla del Mar s/n,
E-30.202, Cartagena, Murcia, Spain
E-mail: mae.requena@upct.es

Abstract: In this work, a learning architecture based on neural networks has been employed for modelling the electric field pattern along an axis of a multimode microwave-heating cavity that contains dielectric materials. The multilevel configuration of this architecture, based on Radial Basis Functions (RBF) and polynomial structures, allows the fitting of the electric field as a function of the dielectric parameters (i.e. $\varepsilon^* = \varepsilon' - j\varepsilon''$) along one axis ($x$) of the cavity as well as inside the sample. In the learning stage, different samples have trained the neural architecture, by means of the mapping between $(\varepsilon', \varepsilon'')$ and the absolute value of the electric field pattern, generated with a 2D simulation platform based on the Finite Elements Method (FEM). The results obtained with conventional samples, such as polyester, epoxy, silicon crystal or beef steak, show that the proposed neural model is able to accurately predict the electric field spatial distribution under appropriate training processes.

Keywords: electric field estimation; learning-based predictive system; microwave-assisted applications; microwave-heating oven; neural network modelling.

Reference to this paper should be made as follows: Pedreño-Molina, J.L. and Monzó-Cabrera, J., Pinzolas, M. and Requena Pérez, M.E. (0000) 'A new predictive neural architecture for modelling electric field patterns in microwave-heating processes', *Int. J. Materials and Product Technology*, Vol. 00, Nos. 0/0, pp.000–000.

Biographical notes: J.L. Pedreño-Molina was born in Cartagena (Murcia), 1969. He received his BSc in 1984 from the Technical University of Madrid, Spain (UPM) and a PhD in Neurotechnology, Control and Robotics in 2000. He is Associate Lecturer of Telecommunication Engineering at the Technical University of Cartagena (UPCT), Spain. Since 1999, he has worked in the Department of Information Technologies and Communications at UPCT. His research interests are in signal processing applied to optimisation and control of nonlinear systems, and modelling based on neural networks with applications to robotics and drying processes.

J. Monzó-Cabrera was born in Elda (Alicante), Spain, in January 1973. He received Dipl Ing and PhD degrees in Telecommunications Engineering from the Universidad Politécnica de Valencia, Valencia, Spain, in 1998 and 2002, respectively. From 1999 to 2000, he was a research assistant with the Microwave Heating Group (GCM). In 2000, he joined the Departamento de Tecnologías de la Información y las Comunicaciones, Universidad Politécnica de Cartagena, Cartagena, Spain, as an associate lecturer. His current research areas cover microwave-assisted heating and drying processes, microwave applicator design and optimisation and numerical techniques in electromagnetics.

M. Pinzolas earned his MSc degree in Physics from the University of Saragossa (1992) and his PhD in Industrial Engineering from the Public University of Navarre (1997). He has been Assistant Lecturer at the Public University of Navarre, Visiting Researcher at the University of Reading and currently he is Senior Lecturer at the Technical University of Cartagena. His main research interests are related to neural network learning and applications and with computer vision. He is a member of the IEEE and of the Spanish branch of IFAC.

María E. Requena-Pérez was born in Alicante, Spain. She received a Dipl Ing degree in Telecommunications Engineering from the Universidad Politécnica de Valencia, Valencia, Spain. In 2000, she joined the Department of Information Technologies and Communications. Her current research areas cover microwave-assisted heating and drying processes, microwave applicator design and optimisation and numerical techniques in electromagnetics.

1 Introduction

Microwave heating is a technique that is employed for the processing of a great variety of industrial materials, such as leather, paper, wood, food, textile, rubber and resins (Meredith, 1988; Metaxas and Meredith, 1983; Monzó-Cabrera et al., 2002). In these processes, the knowledge of the electric field distribution within the material is a basic question, since it indicates the way in which the material will be heated, showing the so-called 'hot spots' and the regions that heat at a lower rate. Traditionally, the computation of the electric field within microwave heating applicators has been based on the resolution of Maxwell's equations and the so-called wave equation (Chow-Ting-Chan and Reader, 2000). Several numerical methods can be employed to solve Maxwell's equations in microwave ovens although the most

common methods used are Finite Differences in the Time-Domain (FDTD) and the Finite Elements Method (FEM). Microwave heating applications using these methods can be found in Kopyt and Celuch-Marcysiak (2003) and Sundberg et al. (1996), respectively. However, the main drawbacks for these methods are the long computing times, mainly for three-dimensional (3D) structures and the need of new simulations when the properties of the material, such as permittivity, size and shape, change (Chow-Ting-Chan and Reader, 2000). All these aspects are particularly important in real microwave-heating processes in which the material features may change during the heating period due to the sample temperature increase and its internal structure variations.

On the other hand, the models based on learning architectures, such as Artificial Neural Networks (ANN), are able to deal with the relationship between these material features and the electric field deposition for a fixed applicator. The use of ANN implies that, after the training stage, these methods are able to accurately predict the electric field distribution within the material to be processed without turning back to the resolution of Maxwell's equations which drastically reduce computing times (Kuroda and Kim, 2002; Mittal and Zhang, 2000).

These learning capabilities have led several authors to use ANN for the resolution of complex electromagnetic problems, such as permittivity measurements (Eves et al., 2004), microwave structure optimisation (Murphy and Yakovlev, 2003; Watson and Gupta, 1997), microwave devices modelling (Creech et al., 1997; Patnaik et al., 1997; Vai et al., 1997) and improvement of the calibration procedures (Jargon and Gupta, 2001; Jargon et al., 2000a,b). Thus microwave devices can be modelled from an ANN point of view. An example of an application of this structure for solving inverse problems in microwave cavities can be found in Pedreño-Molina et al. (2004).

In this work, the x-axis has been considered as the axis of the magnetron. We propose an ANN architecture that is able to learn and predict, for any dielectric material the module of electric field curves as a function of permittivity (dielectric constant (ε') and the loss factor (ε'')) and distance from the power source, i.e. $\mathrm{E}(x, \varepsilon', \varepsilon'')$. Thus, the learning capabilities of ANN have been applied for modelling the relationship between the spatial dependence of both the sample and cavity electric field spatial distribution for a microwave heating applicator along the x-axis. The analysis of the error has been made as function of several parameters of the neural networks involved in order to study the sensitivity and robustness of the proposed neural architecture. When compared with numerical methods for the estimation of electric field distribution in the described scenario, the proposed architecture avoids the knowledge of the physical model of the process, since in this case it is rather complex. In fact, the final structure has been designed by means of a simple mathematical model, based on matrix products, which can be implemented in dedicated hardware devices (FPGA or DSP) which have the possibility of real-time working. Although the proposed architecture has been tested over 2D simulation platforms, it can be easily extended to predict the electric field pattern in 3D real applications. An example of the application of this model to a problem which is more difficult to solve with traditional methods, is the inverse problem in microwave heating structures described in Pedreño-Molina et al. (2004).

2 Simulation set-up

Figure 1 illustrates the geometry of the 2D multimode microwave-heating cavity used in our electric field pattern modelling, in which ideal metallic walls are assumed. In this scheme, the sample is placed in a fixed position along the x axis and it is centred with respect to the magnetron and the y-axis cavity length.

Figure 1 Scheme of the partially filled microwave oven

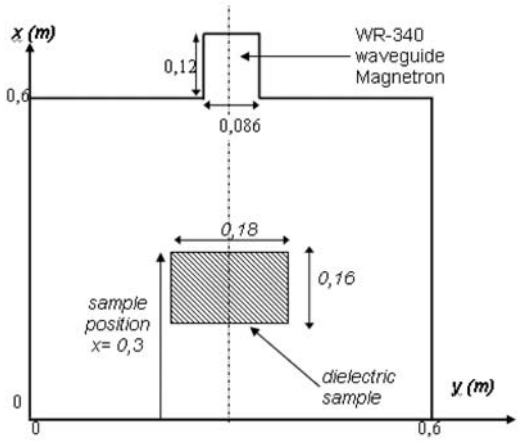

Complex permittivity of the dielectric load has been varied during the training. For this purpose, the fundamental TE_{10} mode is excited in a standard WR-340 waveguide at 2.45 GHz and the module of the complex electric field has been calculated along the x-axis for each simulation. The electromagnetic problem has been solved in the frequency domain with the aid of the vector wave equation

$$\nabla^2 \mathbf{E} + \omega^2 \mu \varepsilon \mathbf{E} = 0, \tag{1}$$

where $\mathbf{E}$ is the vector electric field, ω is the angular frequency, μ is the permeability and ε is the complex relative permittivity of the medium, considering, in this study, non-magnetic materials.

FEM has been used to solve this equation for each electric field component, by using the variational formulation as indicated in the Partial Differential Equation Toolbox (1996). The MATLAB 6.0^{TM} PDE Toolbox has been used to discretise the 2D domain and to obtain the electric field distribution inside the partially filled multimode cavity. The PDE Toolbox supplies several tools so that the user can define a PDE problem (definition of 2D regions, boundary conditions, and PDE coefficients), numerically discretise and solve the PDE equations, produce an approximation to the solution and, finally, visualise the results.

3 Two-level neural architecture design

The proposed neural architecture is configured in a novel two-level structure that combines the accuracy of the neural networks based on radial basis functions (RBF) (Broomhead and Lowe, 1988) and the algebraic capabilities of polynomial matrix equations.

During the learning stage, the proposed neural architecture is trained from electric field intensity curves, $\mathrm{E}(x)$, generated with a 2D simulation platform based on MATLAB PDETool. Thus, numerical scenarios with different dielectric materials are randomly generated and characterised by their specific ε' and ε'' values. These materials are considered for obtaining the electric field distribution along the x-axis and for training the proposed ANN structure.

Previous analyses of the electric patterns' evolution for different materials have been performed in this work by using the PDETool. This has allowed the analysis of the influence of the loss factor (ε'') on the electric field pattern behaviour within the sample and in the oven. Due to the great sensibility of the $\mathrm{E}(x)$ curves versus the ε'' observed, three different sample categories have been considered during the learning procedure in order to improve the accuracy of electric field modelling both in the cavity and inside the sample. Hence, the variation range for ε'' has been subdivided nto three intervals: (1.5–20), (0.75–1.5) and (0.3–0.75), corresponding to high (*H*), imedium (*M*) and low (*L*) losses, respectively, because different behaviours are detected for $\mathrm{E}(x)$ inside the sample. They must be characterised by different learned matrices.

In microwave-assisted drying and heating processes the evolution of the electric field in any direction of the cavity ($\mathrm{E}(x)$ vector in this case), both inside and outside the sample, is highly dependent on the dielectric characteristics of the material considered (ε' and ε'') (Chow-Ting-Chan and Reader, 2000). Additionally, $\mathrm{E}(x)$ curves present nonlinear variations which are very dependent on the material permittivity. In order to overcome the problems associated with the nonlinear behaviour of the electric field pattern, the sensibility of $\mathrm{E}(x)$ inside the sample with respect to ε'' and the generation of $\mathrm{E}(x)$ from only two parameters, this architecture has been implemented with two interconnected levels and three sample categories for the learning procedure. The scheme of the proposed neural architecture is shown in Figure 2.

Figure 2 General scheme of the proposed neural architecture. The RBF neural network in Level 1 generates the estimated temperature $\tilde{E}(x)$ from ε' and ε''

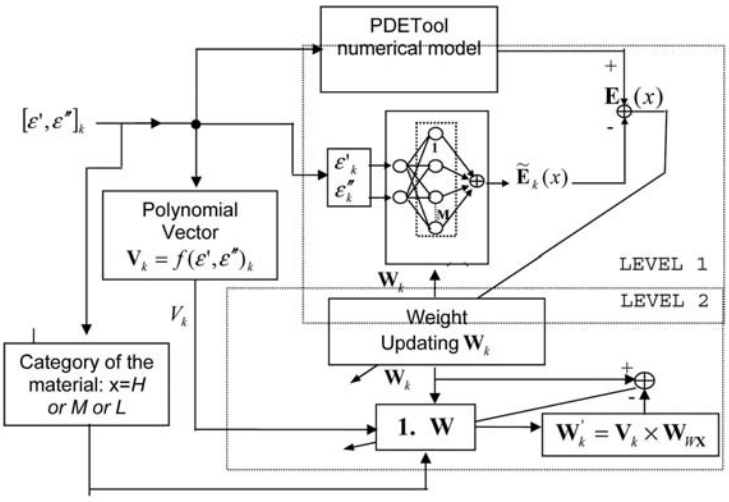

Note: The polynomial network in Level 2 establishes the mapping between the neural weights in Level 1 and the weights of the polynomial network in Level 2 for the three types of materials considered

A neural network based on RBF has been selected for electric field identification in Level 1, while a polynomial relationship has been employed in Level 2 for mapping the RBF neuron weights obtained from each training trial over the input variables ε' and ε''.

When the final neural weights matrix is generated, the predictive capabilities of the ANN structure can be applied to polymers such as epoxy, polyester or silicon, and the results validated by using Maxwell's equations.

4 Learning and modelling equations

In the first level of the ANN architecture, a solution for the interpolation of the nonlinear function $\mathrm{E}(x)$ for each k pair $[\varepsilon', \varepsilon'']_k$ involved in the training procedure, is achieved by learning the Gaussian functions neurons weights of the RBF networks. Then, in the second level the neuron weight vector for the kth trial, $\mathbf{W}_k$, is correlated with the input variables' set $[\varepsilon', \varepsilon'']_k$, which generated $\mathrm{E_k}(x)$ at the 2D simulation platform. By considering all the learning trials, this mapping finally generates the neuron weights matrix, $\mathrm{W_W}$, which is obtained by a polynomial network whose coefficients are learned in this level.

Due to the great influence of ε'' on the generation of $\mathrm{E}(x)$ and the nonlinear behaviour of electric field patterns, a segmentation in three categories for the training interval for ε'' has been made. This implies the generation of three different neuron weight matrices $\mathrm{W_{WH}}$, $\mathrm{W_{WN}}$ and $\mathrm{W_{WL}}$, whose intervals for ε'' are (1.5–20), (0.75–1.5) and [0.3–0.75), respectively. For ε', the training interval has been considered (1–50) for all the categories.

The function $\mathrm{E}(x)$ is considered to be restricted to the one-dimension interval, $x \in [0 \ldots 0.6]$. T equally spaced samples have been considered in this interval for the absolute value of the electric field for the design of the RBF network in Level 1. RBFs are supervised neural networks (Broomhead and Lowe, 1988) whose structure provides a solution to the local interpolation of nonlinear functions, such as $\mathrm{E}(x)$. The structure of the RBF requires defining Gaussian functions whose centres are distributed along the interval of definition for the function to be fit. An appropriate adjustment for the standard deviation of each Gaussian function is important to ensure a good interpolation for $\mathrm{E}(x)$. Thus, in the first level of the proposed architecture, the x interval, in which the electric field pattern is defined, is divided into M intervals. Each M interval is associated with one RBF neuron in order to project the T points of $\mathrm{E}(x)$ onto the M RBF neurons ($M < T$). In the learning stage of the RBF neural network, N trials for the training are considered for the three specified categories.

Consequently, Level 1 provides a solution to the interpolation of each nonlinear function $\mathrm{E}(x)$ along the internal dimension of the sample and the rest of the cavity. For the k pair ($k = [1, \ldots, N]$, (with N being the number of trials during the learning stage) of input variables $[\varepsilon', \varepsilon'']_k$, the estimation of $E_k(x)$ is given by:

$$\tilde{E}_k(x) = \sum_{j=1}^{M} w_{jk} \cdot e^{\left(-\frac{(x-\mu_j)^2}{\sigma^2}\right)} = \sum_{j=1}^{M} w_{jk} \cdot \phi_{jk}(x) \tag{2}$$

where $\phi_{jk}(x)$ is the j Gaussian radial function, μ_j and σ are the centre and the constant standard deviation of $\phi_{jk}(x)$, and w_{jk} is the value of the weight associated with $\phi_{jk}(x)$ in the kth trial. The μ_j parameters are the M centres equally spaced along the x axis from 0 to 0.6 m. Rewriting the Equation (2) into a matrix notation, results in:

$$\tilde{E}_k(x) = \mathbf{W}_k \cdot \mathbf{\Phi}_k(x)^T \tag{3}$$

where $\mathbf{W}_k$ is the $1 \times M$ dimension vector containing the RBF neuron weights for the kth trial and $\phi_k(x)$ is the vector whose elements are the M Gaussian functions with uniform distribution of the centres and constant standard deviation. The expression (3) is computed for all the N trials considered in the three material categories, and each $\mathbf{W}_k$ vector is learned by using the Least Mean Squared (LMS) algorithm (Haykin, 1996) to minimise the error cost function described in the next equation:

$$H_k = \sum_{x=1}^{T} \left(\mathbf{E}_k(x) - \tilde{\mathbf{E}}_k(x)\right)^2. \tag{4}$$

As a conclusion, the application of the RBF neural network to the estimation of $\tilde{\mathbf{E}}_k(x)$ permits us to obtain the optimal values for w_{jk} from functions generated by the 2D model based on FEM and without restrictions for the dielectric properties of the material. The second level establishes the relationship between $\mathbf{W}_k$ and the $\mathbf{V}_k$ vector, for all the M neurons and all the k trials, by means of the matrix $\mathrm{W_W}$. The $\mathbf{V}$ vector corresponds to the input for the second network, which has been designed by means of a polynomial relationship between $\mathbf{V}_k$ and $\mathbf{W}_k$. The components of this vector are dependent on both ε' and ε'', which are the input variables for the heating process. The dependence of each component of the vector $\mathbf{W}_k$ with respect to ε' and ε'' is computed by means of a polynomial matrix whose order is established by means of the $\mathbf{V}_k$ vector as:

$$\mathbf{V}(\varepsilon', \varepsilon'') = \left\{1, \varepsilon', \varepsilon'', \varepsilon'^2, \varepsilon''^2, \varepsilon'\varepsilon'', \varepsilon'^3, \varepsilon''^3, \varepsilon'^2\varepsilon'', \varepsilon'\varepsilon''^2\right\}. \tag{5}$$

In this expression, a third order dependence of each neuron weight with respect to each variable is represented. Because the Gaussian functions are represented with negative exponentials, each component of the $\mathbf{W}_k$ vector is used for fitting a small interval for the $\mathrm{E}(x)$ function. This is possible, by appropriately adjusting the σ parameter of each basis function. Thus, a polynomial dependence is able to locally establish the relationship between each neuron weight and the ε' and ε'' variables.

By considering the N learning trials, the mapping between $\mathbf{W}_k$ and $\mathbf{V}_k$ generates the matrix $\mathbf{W_W}$, whose dimension is equal to $P \times M$, with P being the length of the $\mathbf{V}$ vector according to Equation (5). The weights of the $\mathbf{W_W}$ matrix are obtained by minimising the quadratic error between $\mathbf{W}_k$ and $\mathbf{W}'_k = \mathbf{V}_k \cdot \mathbf{W_W}$.

By applying the polynomial network to the RBF neuron weights, $\tilde{E}(x)$ can be generated, by considering the three described categories for the materials, from the input variables $[\varepsilon', \varepsilon'']$ by means of the next expression:

$$\tilde{\mathbf{E}}(x, \varepsilon', \varepsilon'') = \mathbf{W} \cdot \mathbf{\Phi}(x, \mu_i, \sigma)^T = \mathbf{V}(\varepsilon', \varepsilon'') \cdot \mathbf{W_{WX}} \cdot \mathbf{\Phi}(x, \mu_i, \sigma)^T \tag{6}$$

where $\mathrm{W_{WX}}$ is evaluated as $\mathrm{W_{WH}}$, $\mathrm{W_{WM}}$ and $\mathrm{W_{WL}}$ depending if the material is considered as a high, medium, or low loss dielectric.

The components of each W_{WX} matrix are learned by following the linear regression algorithm for the matrices shown in the following equations.

$$\mathbf{S} = \begin{bmatrix} \varepsilon'_1 & \varepsilon''_1 \\ \varepsilon'_2 & \varepsilon''_2 \\ \vdots & \vdots \\ \varepsilon'_N & \varepsilon''_N \end{bmatrix} \tag{7}$$

$$\mathbf{R} = \begin{bmatrix} w_{11} & w_{12} & \cdots & w_{1M} \\ w_{21} & w_{22} & \cdots & w_{2M} \\ \vdots & \vdots & & \vdots \\ w_{N1} & w_{N2} & \cdots & w_{NM} \end{bmatrix} \tag{8}$$

$$\mathbf{W_W} = \left(\mathbf{S}^T \times \mathbf{S}\right)^{-1} \times \mathbf{S}^T \times \mathbf{R} \tag{9}$$

where $\mathbf{R}$ and $\mathbf{S}$ represent the dielectric parameters and the neuron weights for $\mathbf{W_W}$, respectively.

The analysis of the normalised quadratic error will permit a appropriated adjustment for the neural architecture in order to decrease the number of neurons $(M \times P)$ in the final matrix $\mathbf{W_W}$. In this last case, the values for P by considering a third, second or lineal order are 10, 6 and 3, respectively, while the values for M will be set to 10, 20 and 60.

5 Results

The scheme of the neural architecture, whose parameters are shown in Figure 2 and Equations (3)–(11) has been used for learning and predicting electric field patterns along the x axis, when the dielectric parameters of the sample are known. The two-level design and the sample loss classification involved in the proposed neural architecture allow the modelling of the electric field in both the sample $(x \in [0.14-0.3])$ and the cavity $(x \in [0-0.14], [0.3-0.6])$. During the learning stage, random values for the input parameters ε' and ε'' have been generated and different $\mathbf{E}(x)$ curves were obtained by means of the numerical 2D PDETool simulator. In this learning stage 500, 300 and 300 trials have been carried out for materials with high, medium and low losses, respectively. A frequency of 2.45 GHz has been used for all the simulations. The numerically computed $\mathbf{E}(x)$ curves have been obtained by sampling the x axis with 0.0025 m slots from 0 to 0.6 m. This implies $T = 233$ patterns for $\mathbf{E}(x)$.

For all the Gaussian functions of the RBF neural network, $\mu_i = T \cdot i/M$ $(i \in [1, M])$ and $\sigma = T/M$ have been defined. The performance of the proposed architecture for the prediction of $E(x)$ from the input parameters (ε' and ε'') has been evaluated for several materials with very different loss factors. In Figures 3–6, the absolute value of the electric field pattern along the x-axis for epoxy (3.78–j0.91), polyester (4.66–j0.4), silicon crystal (3.78–j4) and beef steak (40–j12) are shown. The

dielectric characteristics for these materials have been collected for 2.45 GHz from the data provided in Metaxas and Meredith (1983). In these figures, the predicted behaviour of the proposed ANN model is represented as a function of M in Level 1, by considering three values, namely 10, 20 and 60. In Figures 3–6 a third order polynomial structure has been used in Level 2. The position of the sample is represented as a segment in order to distinguish this area from the rest of the cavity.

Figure 3 ANN electric field prediction: epoxy sample (medium losses)

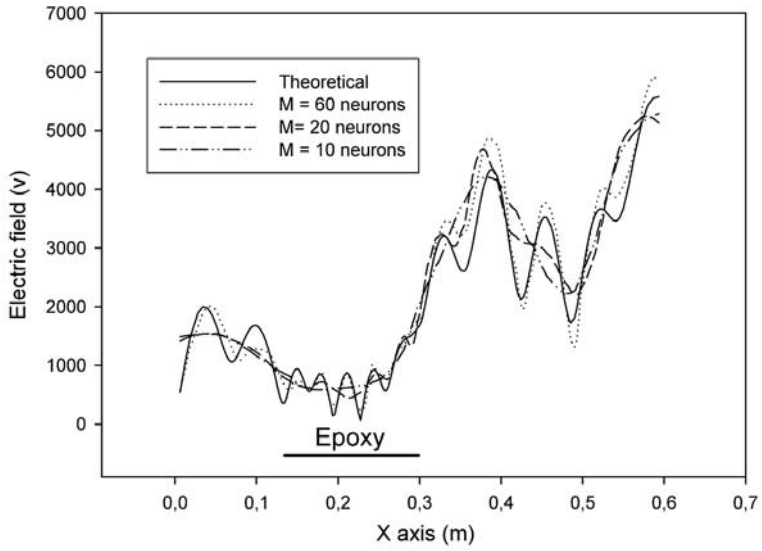

Figure 4 ANN electric field prediction: polyester sample (low losses)

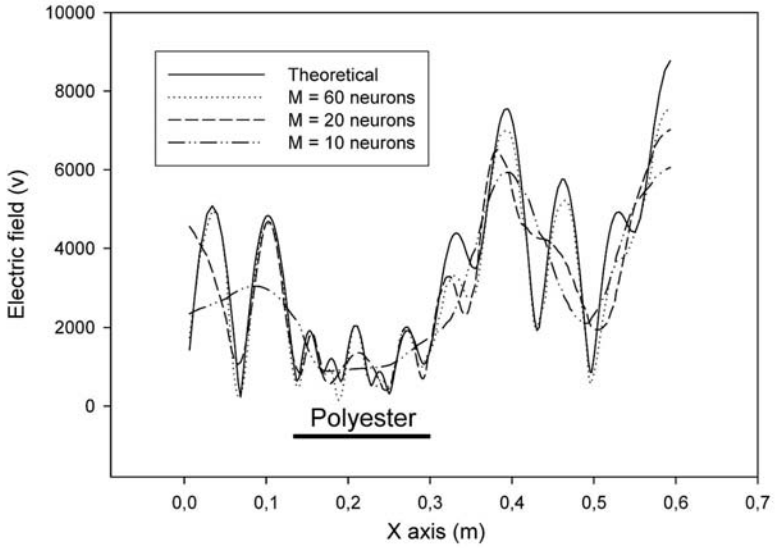

Figure 5 ANN electric field prediction: silicon sample (high losses)

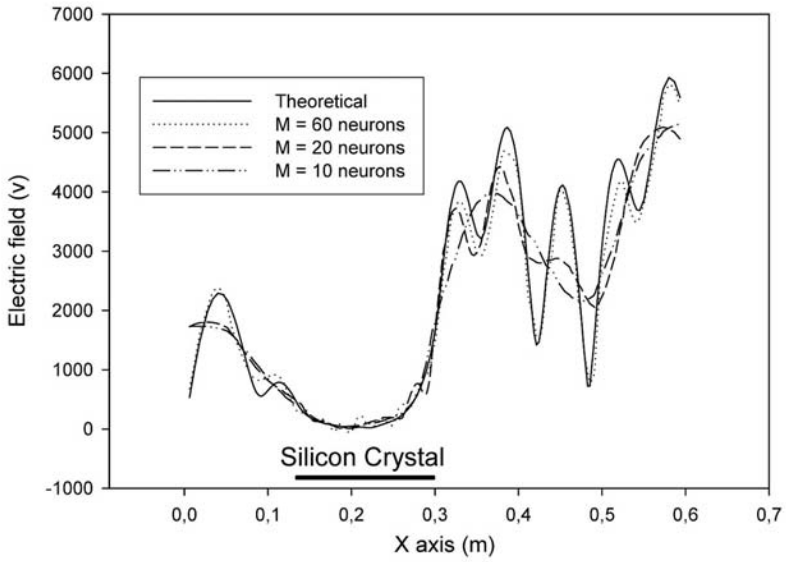

Figure 6 ANN electric field prediction: beef steak sample (high losses)

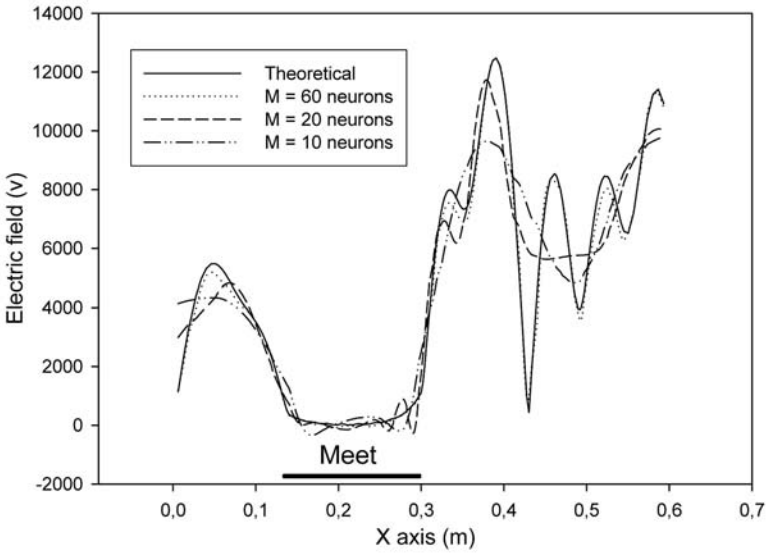

From Figures 5 and 6, one can conclude that the electric field's spatial distributions within the high-loss samples, present a similar uniformity within the sample. Indeed the electric field is more intense at the sample edges than at the sample centre. For these cases, the $\mathbf{W_{WH}}$ matrix permits the matching of the electric field along the whole cavity, including the sample.

However, when the loss factor decreases, the nonlinearity of the electric field within the sample increases. This is observed in Figures 3 and 4 where the electric field shows more oscillations than in Figures 5 and 6. Thus, this justifies the learning

of new matrices for the other materials considered with medium and low losses. The sensibility of $\mathbf{E}(x)$ with respect to ε'' is observed within the sample, while for the rest of the x-axis, electric field patterns presents a similar behaviour for all the cases.

From the evolution of the estimated curves with respect to the number of RBF neurons (M), one can deduce that a higher value for M implies a more accurate performance for the neural model. Values greater than 60 present very small differences in the error function but this implies increasing the computation of the $\mathbf{W_W}$ matrix.

In order to analyse the behaviour of the neural architecture with respect to the estimated order for the polynomial structure, different orders from 1 to 3 have been used for training the polynomial network, being $M = 60$ in Figures 7–10. Furthermore, from the good matching of both PDE and ANN curves, one can conclude that the use of a third degree polynomial model in Level 2 provides sufficient final precision for the $M \rightarrow 2$ projection in each interval.

Figures 7–10 show the estimated electric field pattern obtained for the same four samples: epoxy, polyester, silicon crystal and beef steak, respectively. The new dimensions for the $\mathbf{W_W}$ matrix are, in this case, 180, 360 and 600, for lineal-, second- and third-order polynomial structures in Level 2, respectively.

As can be observed in Figures 7–10, a third order for the polynomial network is good enough to achieve an acceptable matching for $\mathbf{E}(x)$. Furthermore, in these figures the differences between the second- and third-order performance are not very important for electric field values outside the dielectric sample. The second order for the polynomial structure supposes a great advantage in order to decrease the number of neurons in the final neural architecture. However, the performance difference between orders 2 and 3 can be observed in terms of the electric field evolution inside the sample. From these data, one can conclude that a third-order polynomial structure is necessary in Level 2 of the proposed ANN architecture if an acceptable accuracy is to be obtained, even within the dielectric sample.

Finally, in order to test the accuracy of the proposed architecture with samples in the three considered categories, several comparisons have been carried out by using the PDETool for $\mathrm{E}(x)$, and its prediction $\tilde{E}(x)$ by means of the neural architecture. Then, a normalised error mean parameter, calculated inside the sample and in the whole cavity, has been obtained in order to validate the matching performance. The error indicators have been defined for the electric field patterns both in the cavity, $Error_C$, and in the sample $Error_S$ as follows:

$$Error_C = \left(\frac{E_C(x) - \tilde{E}_C(x)}{maximum_C} \right)^2 * 100(\%) \tag{10}$$

$$Error_S = \left(\frac{E_S(x) - \tilde{E}_S(x)}{maximum_S} \right)^2 * 100(\%) \tag{11}$$

where the subscripts, C and S, indicate that the estimation is made along the cavity or the sample, respectively, and the *maximum* parameter indicates the maximum value for the electric field provided by the PDE Toolbox in the considered interval for the cavity or the sample. Table 1 shows the $Error_C$ and $Error_S$ values for different dielectric samples. From this data one can conclude that the error increases when the loss factor decreases, because the electric field intensity within the sample grows as well as the oscillations within the cavity.

Figure 7 ANN electric field pattern prediction versus the order of the polynomial network: epoxy sample (medium losses)

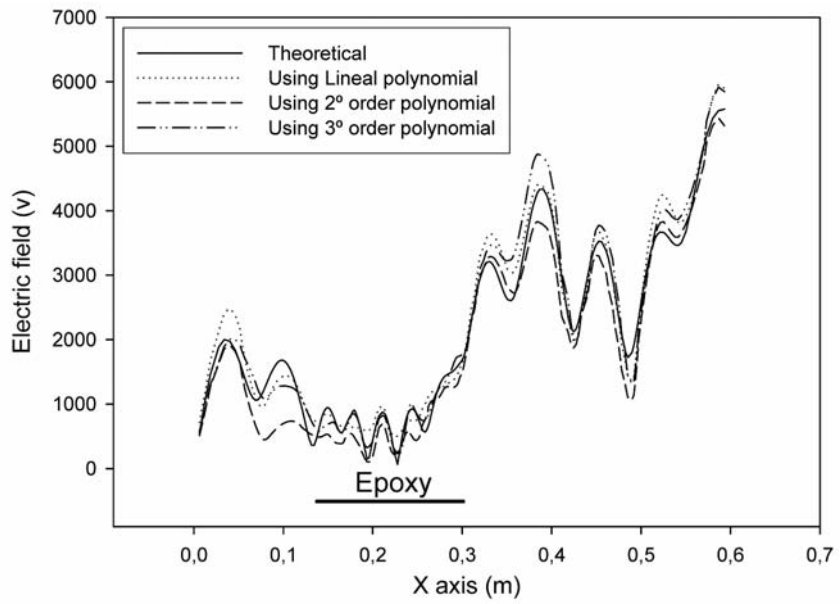

Figure 8 ANN electric field pattern prediction versus the order of the polynomial network: polyester sample (low losses)

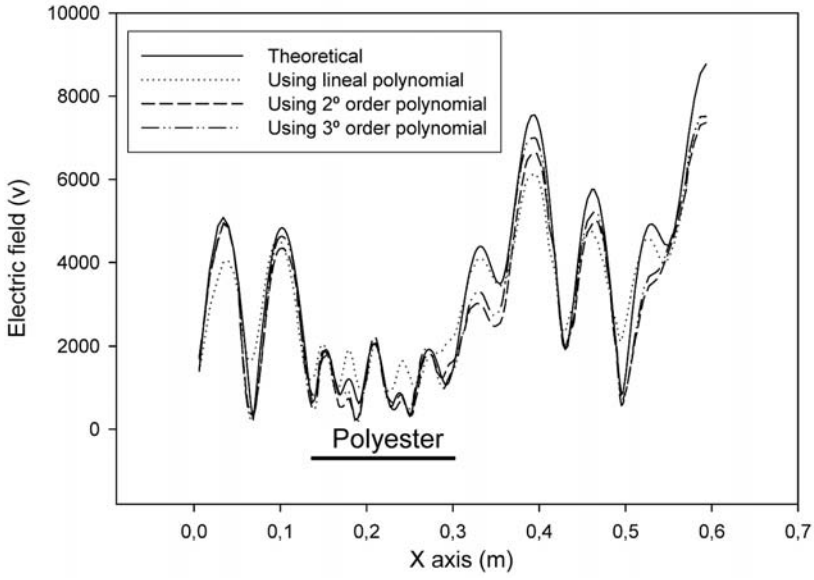

Figure 9 ANN electric field pattern prediction versus the order of the polynomial network: silicon crystal (high losses)

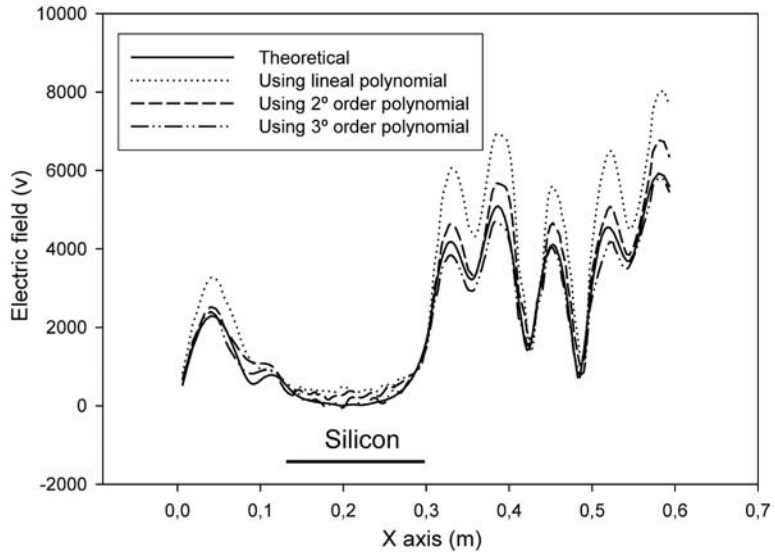

Figure 10 ANN electric field pattern prediction versus the order of the polynomial network: beef steak sample (high losses)

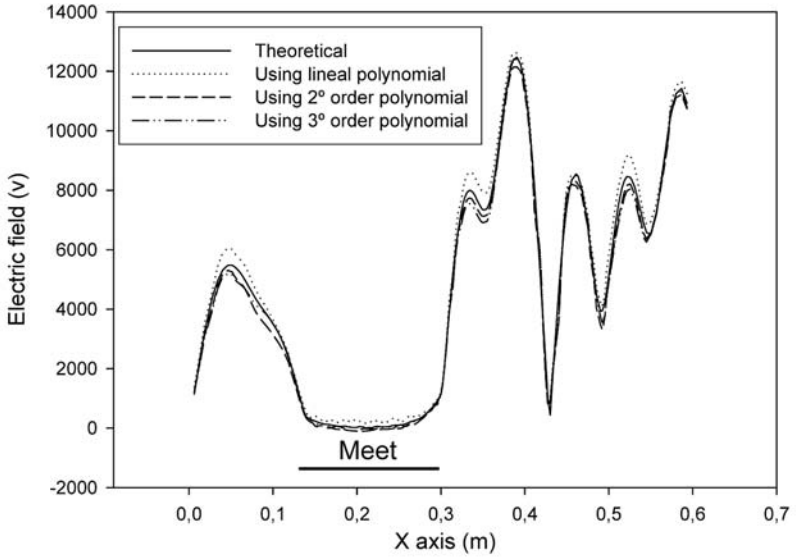

Table 1 $Error_C$ and $Error_S$ for samples different from the training set

$\varepsilon' - j\varepsilon''$	*30–j20*	*15–j6*	*25–j9*	*20–j15*	*9–j1.5*	*2–j0.9*	*6–j1*	*4–j0.7*	*2–j0.6*	*4–j0.45*	*1–j0.3*
$Error_C$ (%)	0.10	0.09	0.08	0.12	1.17	0.19	0.57	0.24	0.14	0.90	3.04
$Error_S$ (%)	1.60	0.30	0.62	0.75	5.46	1.55	1.54	1.52	1.23	2.14	4.49

6 Conclusions

In this paper, a novel architecture based on neural networks has been applied for modelling electric field patterns in multimode microwave-heating ovens. The design of a two-level neural architecture is able to predict the evolution of the electric field along one direction inside the cavity from only two input parameters, namely ε' and ε''. This two-level architecture and the inclusion of three different learning categories, depending on ε'', have allowed good matching behaviour without restrictions for the dielectric characteristics of the samples. The results are obtained by interconnecting the adaptive characteristics of the RBF with the algebraic tools of polynomial relationships. Important advantages of the proposed learning-based model with respect to conventional electromagnetic models, based on differential equations, are the capabilities for prediction in dynamic environments, the reduction of computational resources, the generation of a simple mathematical model based on matrix products, and the lack of need for precise knowledge of the heating process. Additionally, the adaptive capabilities of neural networks could be used to extend the excellent performance of the proposed model to other regions of the cavity, in order to estimate the evolution of the electric field.

The results obtained have been focused on conventional materials such as epoxy, polyester, silicon crystal or meat, and a good approximation of the electric field both inside the sample and the cavity has been obtained. Although the direction for the electric field modelling has been considered in this work the x-axis, it must be pointed out that the proposed architecture is valid for any direction within the cavity. Thus, the extension of the learning procedures to other cavity directions could generate the two-dimensional modelling of the electric field patterns.

As a conclusion, this work provides a general learning structure able to closely predict the relationship between the electric field function inside the cavity and dielectric properties of samples and the medium. Additionally, this technique allows fast computation times, and provides a predictive structure able to adapt its response to the intrinsic features of the material.

References

Broomhead, D.S. and Lowe, D. (1988) 'Multivariable functional interpolation and adaptive networks', *Complex Systems*, Vol. 2, pp.322–355.

Chow-Ting-Chan, T.V. and Reader, H.C. (2000) *Understanding Microwave Heating Cavities*, Boston & London: Artech House.

Creech, G.L., Paul, B.J., Lesniak, C.D., Jenkins, T.J. and Calcatera, M.C. (1997) 'Artificial neural networks for fast and accurate EM-CAD of microwave circuits', *IEEE Trans Microwave Theory Tech*, Vol. 45, pp.794–802.

Eves, E., Kopyt, P. and Yakovlev, V.V. (2004) 'Determination of complex permittivity with neural networks and fdtd modeling', *Microwave And Optical Technology Letters*, Vol. 40, No. 3, pp.183–188.

Haykin, S. (1996) *Adaptive Filter Theory*, 3rd edition, New Jersey: Prentice Hall.

Jargon, J.A. and Gupta, K.C. (2001) 'Artificial neural network modeling for improved coaxial line-reflect-match calibrations', *Int J RF and Microwave CAE*, Vol. 11, pp.33–37.

Jargon, J.A., Gupta, K.C. and DeGroot, D.C. (2000a) 'Artificial neural network modeling for improved on-wafer OSLT calibration standards', *Int J RF and Microwave CAE*, Vol. 10, pp.319–328.

Jargon, J.A., Kirby, P., Gupta, K.C., Dunleavy, L. and Weller, T. (2000b) 'Modeling load variations with artificial neural networks to improve on-wafer OSLT calibrations', *Proc 56th ARFTG Conference Digest*, pp.76–88.

Kopyt, P. and Celuch-Marcysiak, M. (2003) 'FDTD modelling and experimental verification of electromagnetic power dissipated in domestic microwave ovens', *J. Telecommunications and Information Technology*, Vol. 1, pp.59–65.

Kuroda, C. and Kim, J. (2002) 'Neural network modeling of temperature behavior in an exothermic polymerization process', *Neurocomputing*, Vol. 43, pp.77–89.

Meredith, R. (1988) *Engineers' Handbook of Industrial Microwave Heating*, London: IEE.

Metaxas, A.C. and Meredith, R.J. (1983) *Industrial Microwave Heating*, London: Peter Peregrinus Ltd, pp.89–120.

Mittal, G.S. and Zhang, J. (2000) 'Prediction of temperature and moisture content of frankfurters during thermal processing using neural network', *Meat Science*, Vol. 55, pp.13–24.

Monzó-Cabrera, J., Catalá-Civera, J.M., Canós, A.J. and De los Reyes, E. (2002) 'Simulation of temperature distributions in pressure-aided microwave rubber vulcanization processes', *J. Microwave Power and Electromagnetic Energy*, Vol. 37, No. 2, pp.73–88.

Murphy, E.K. and Yakovlev, V.V. (2003) 'FDTD-backed RBF neural network technique for efficiency optimization of microwave structures', *Proc. of the 9th AMPERE Conf. on Microwave & RF Heating*, Loughborough, UK, pp.197–200.

Partial Differential Equation Toolbox (1996) For use with MATLAB, *User's Guide*, The MathWorks, Inc. available from: http://www.mathworks.com.

Patnaik, A., Mishra, R.K., Patra, G.K. and Dash, S.K. (1997) 'An artificial neural network model for effective dielectric constant of microstrip line', *IEEE Trans. Antennas Propagation*, Vol. 45.

Pedreño-Molina, J.L., Monzó-Cabrera, J. and Sánchez-Hernández, D. (2004) 'A new predictive neural architecture for solving temperature inverse problems in microwave-assisted drying processes', *Neurocomputing*, Vol. 64, pp.521–528.

Sundberg, M., Risman, P.O., Kildal, P.S. and Ohlsson, T.O. (1996) 'Analysis and design of industrial microwave ovens using the finite difference time domain', *J. Microwave Power and Electromagnetic Energy*, Vol. 31, No. 3, pp.142–157.

Vai, M., Wu, S., Li, B. and Prasad, S. (1997) 'Creating neural network based microwave circuit models for analysis and synthesis', *Proc Asia Pacific Microwave Conf*, Hong Kong, pp.853–856.

Watson, P.M. and Gupta, K.C. (1997) 'Design and optimization of CPW circuits using EM-ANN models for CPW components', *IEEE Trans. Microwave Theory Tech.*, Vol. 45, pp.2515–2523.